

Questions concerning the form taken by the charge-density wave and the accompanying periodic-structural distortions in $2H$ -TaSe₂, and closely related materials

John A. Wilson

Bell Laboratories, Murray Hill, New Jersey 07974

(Received 31 October 1977)

An attempt has been made to understand the detailed form and phasing taken by the periodic-structural distortions (PSD) as developed in the various d^1 - d^0 charge-density-wave (CDW) bearing materials. The diagrammatic mode of presentation which is used facilitates insight into the forces at work at the unit-cell level. In the fully investigated case of the $2H$ structure, with its trigonal prismatically coordinated sandwiches, these are able to modify substantially the simple relationship between PSD and CDW. The proposed phasing of the CDW in the case of $1T$ -TaSe₂ ($1T$ -TaSe₂) goes against recent interpretation of the available data, and a revised interpretation of that data is given. The two PSD's reported for NbTe₂ have for the first time been brought satisfactorily into the present CDW scheme. $3d^1$ VSe₂ and $3d^0$ TiSe₂ provide interesting and illuminating contrasts in behavior compared with $5d^1$ $1T$ -TaSe₂.

I. INTRODUCTION

Section II relates the observed periodic-structural distortions (PSD) in $2H$ -TaSe₂ to a certain phasing of the coupled charge-density wave (CDW). That phase angle determines the geometry of the charge contour map and also its anchoring upon the commensurate lattice. Section III shows how the phasing of the observed PSD is modified from its "ideal" relation to this specified CDW by nearest-neighbor bonding forces, so that the anion and cation sublattice distortion waves are removed from an antiphase relation to each other and from quadrature to the CDW. Section IV addresses some of the factors involved for PSD and phonons when changes of temperature and pressure are considered in the light of Secs. II and III. Note the characteristics of the charge map and its stability are dependent on the phase relation which the triple-axis phonons hold for each other. Section V uses the above basis to examine the PSD's acquired by TiSe₂, VSe₂, NbTe, and $1T$ -TaS₂. The choice of phase angles is much more limited here in the $1T$ -CdI₂ structure (for a symmetric product) than it was for the $2H$ case. We are led ultimately in $1T$ -TaS₂ to requiring that the presently advanced phasing of the CDW be reversed by π .

As details of the periodic structural distortions associated with charge-density waves have started to be available it is illuminating to try to relate the observed anion and cation sublattice wave phasing to displacive and restraining forces. The former derive from the form of the band structure close to the Fermi level, while the latter are dominated by the short-range bonding forces integrating out from all the occupied band states.

By rendering due account to these details of phasing, amplitude, and polarization, a clarifica-

tion and understanding has been gained of the bases from which further developments can more securely and specifically proceed for the various materials involved.

II. DESCRIPTION OF THE PSD FORMED IN $2H$ -TaSe₂ AND THE RELATED CDW

In $2H$ -TaSe₂ neutron-diffraction experiments¹ determine that near 90 °K the incommensurate CDW-PSD, first developed at 122 °K,² discontinuously becomes commensurate with the parent lattice. The superlattice so "locked-in" takes the form $3a_0 \times 3a_0 \times c_0$ with respect to the parent parameters. There now are 18 molecular units per cell (the original c_0 of the $2H$ cell embracing a two sandwich stacking repeat). The space group of the parent structure was D_{6h}^4 ($P6_3/mmc$), for which proper choice of cell origin is a center of inversion sited between the sandwiches in the Van der Waals gap. For both parent and supercells, the pair of sandwiches will be given the distinguishing titles "upper" and "lower." Figure 1 portrays the parent structure oriented in such a way as to be consistent with the notation of Ref. 3. Note by this criterion none of the elements to Fig. 1 in Ref. 2 are "standard," but require viewing through the paper.

The diffraction results from the superlattice phase indicate a high residual hexagonal symmetry, appropriate to the action of a triple-axis CDW. An intersandwich center of inversion is clearly indicated in the commensurate PSD, as could come only from space groups based on D_{6h} and C_{6h} (containing $\bar{6}$), or D_{3d} and C_{3i} (containing $\bar{3}$). After this center of inversion is made coincident with any one of those structural centers of inversion that earlier defined the origin in the

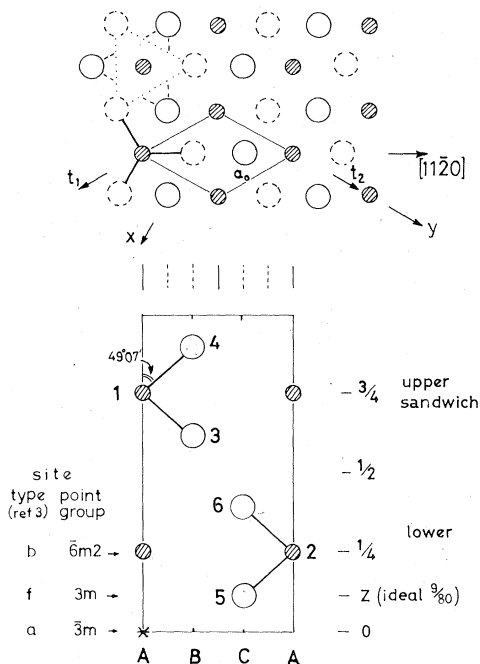


FIG. 1. Structure of $2H\text{-TaSe}_2$ at 300°K , $a_0 = 3.436$ Å, $c_0 = 12.70$ Å, $z = 0.118$ [Ref. 1(b)] (ideal 0.1125, Ref. 11). Ta-Se bond length $\{[c_0(\frac{1}{4} - z)]^2 + (a_0/\sqrt{3})^2\}^{1/2} = 2.597$ Å. Space group D_{6h}^4 ($P6_3/mmc$).

parent structure, the diffraction data were satisfied by the superlattice represented in Fig. 2 and Table I.¹ This structure in fact takes the same space group as did the parent structure (*viz.*, D_{6h}^4), a conclusion recently given support by the number and symmetry of the new Raman modes found to appear with the low-temperature phase.⁴

In order to be able to perceive more clearly the character of the periodic-structural distortion,

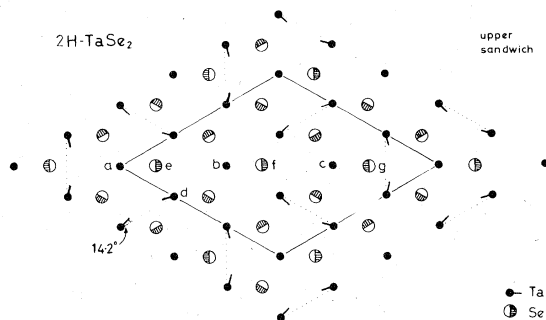


FIG. 2. Displacement pattern in $3a_0$ commensurate PSD of $2H\text{-TaSe}_2$ (upper sandwich) at 5°K . The cation displacements are exaggerated by a factor of 10. The still smaller anion displacements have their directions indicated through the semicircular shading. (The site type labels used here and later are not those of Fig. 1 and Ref. 3.)

the atomic displacements have been broken into their three axial components in Fig. 3. The anion and cation parts to these three condensed modes are shown (for the upper sandwich), these being properly arrayed (see Ref. 2, Appendix), and then phased in accord with the data given in Table I. The modes involved in the PSD are longitudinal, and were shown¹ to take symmetry Σ_1 . Only Σ_1 of the four representations possible in Σ shows predominantly longitudinal character, appropriate for coupling with a CDW. (To a first approximation the atoms should accommodate to a CDW by moving up and down the lines of steepest descent on the charge hills—strictly potential hills, which are by Poisson's equation sinusoidal and in-phase with the charge wave.) Table II gives details of the component and resultant displacements for the four types of Ta atom plus the three types of Se

TABLE I. Neutron-diffraction-deduced amplitudes and phases (see Ref. 1) of individual components (longitudinal) to the triple-axis periodic structural distortions appearing with the commensurate CDW phase of $2H\text{-TaSe}_2$ at 5°K (see Fig. 2). The lower sandwich waves take minus these phase angles, the supercell origin being a center of inversion in the Van der Waals gap.

Direction of displacement	Phasing relative to supercell c axis, of upper-sandwich waves	Amplitude of a single axis component wave ^a (Å)
Ta wave $\perp \vec{c}$	134.2°	0.048
Se wave $\perp \vec{c}$	20.6° (380.6°)	0.009
$\parallel \vec{c}$	164.0°	0.017

^a Experimental difficulties make these lower-limit values; they could be up to a factor of 2 greater [N.B. The Ta phase angle in the table in the preprint version of Ref. 1(b), erroneously carried a minus sign, which has led to some confusion (Ref. 4)].

TABLE II. Upper-sandwich basal-plane displacements in $2H\text{-TaSe}_2$ commensurate PSD at 5°K (see Fig. 3), where $C=0.048 \text{ \AA}$ and $A=0.009 \text{ \AA}$ (see Table I). (N.B. These site-type labels do not have the significance given in Ref. 3 and Fig. 1.)

Atom label and multiplicity	Component displacement vectors at atom	as fraction of single wave amplitude	Resultant displacements as fraction of cation dispersion	in angstroms	as percentage of a_0
Ta	 $m = C \sin(134.2) = C \sin(45.8)$
	 $n = C \sin(134.2 + 240) = C \sin(14.2)$
	 $o = C \sin(134.2 + 480) = C \sin(74.2)$
	 Resultant turned 15.8° from $[11\bar{2}0]$	$C \times 1.50$	1	0.072	2.08
Se	 $p = A \sin(20.6 + 80) = A \sin(79.4)$	$A \times 1.31$	$\frac{1}{6}$	0.012	0.35
	 $q = A \sin(20.6 + 320) = A \sin(19.4)$	$A \times 0.31$	$\frac{1}{25}$	0.003	0.09
	 $r = A \sin(20.6 + 580) = A \sin(40.6)$	$A \times 1.63$	$\frac{1}{5}$	0.015	0.43

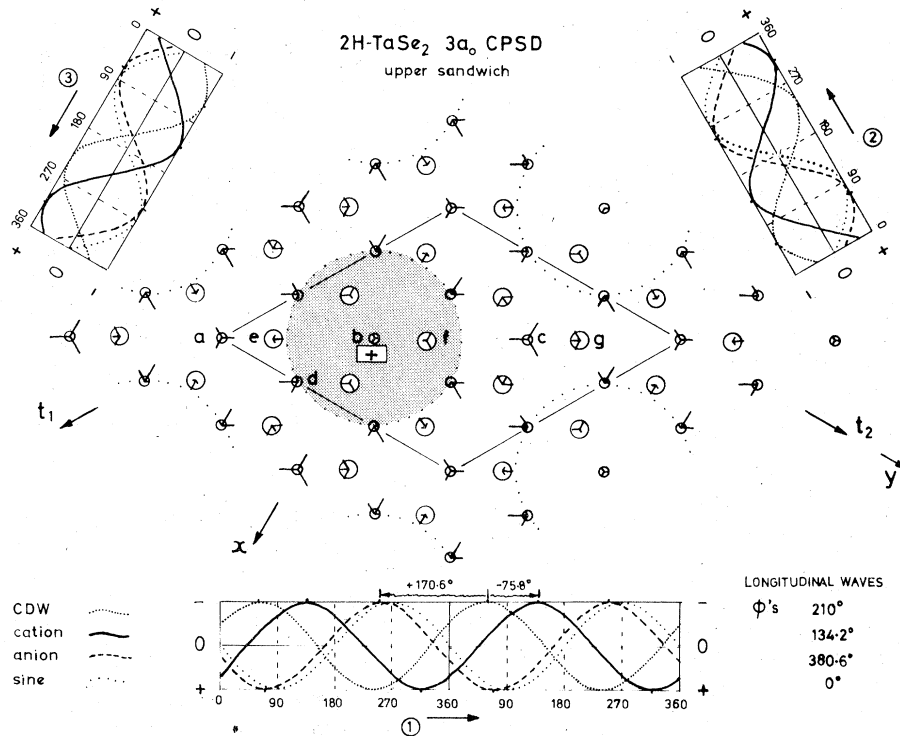


FIG. 3. Displacement pattern of Fig. 2 broken into three axial components. The longitudinal sinusoidal displacement waves take the phasing: cation, $\phi^C = 134.2^\circ$; anion, $\phi^A = 380.6^\circ$. The idealized CDW takes the phasing $\phi = 210^\circ$. With the latter, the shaded area acquires a deficit of negative charge as compared with the unmodulated state. A sine wave ($\phi = 0$) is included for reference. Note cation sites a and c are not equivalent. The wave amplitudes are given in Table I, the displacements in Table II. To obtain the lower sandwich displacements all the phasing signs are changed (waves "inverted").

atom that appear with this supercell. It is to be noted that the largest component for any Se atom (perpendicular to c) is smaller than the smallest component for any Ta atom.

An inspection of Fig. 3 indicates that these dominant movements of the Ta atoms are much as would come in response to a CDW of phase angle relative to the crystallographic origin of close to 210° . 210° waves have been incorporated in Fig. 3. The shading on this figure indicates the regions of charge influx and withdrawal which would follow from such a CDW. The detailed charge contour pattern for a $\phi = 210^\circ$ triple-axis CDW takes the same form as was portrayed in Fig. 31a of Ref. 2 for $\phi = n \times 30^\circ$ (n odd), but now with the positive charge maxima shifted over to crystallographic sites B . In Fig. 4 this charge contour map is shown superposed on the atoms of the symmetry standardized $3a_0$ supercell. What the ideal response of the cations to this CDW would be is here directly apparent. There exists only a 14.2° variance between the observed phase angle of the PSD and its idealized quadrature with this CDW. In Fig. 5 we display the ideal cation response associated with a 210° triple CDW, and in addition show for the anions their ideal response, in antiphase to the cation displacement wave. In Fig. 3 we see the anion wave in fact lay 66.4° beyond antiphase with the observed cation wave, and so $66.4^\circ + 14.2^\circ$

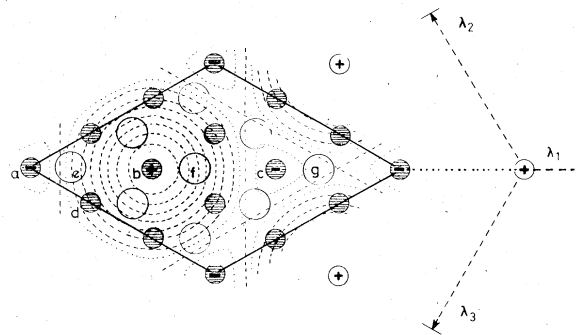


FIG. 4. For symmetric triple-axis CDW's, the spot of common phasing that exists we there designate location A , and term the "phase origin." It acquires the limiting amplitude of $+3$ units when the common phase is (in sine terms) $\phi = 90^\circ$. All other symmetric (i.e., $\phi_i = \phi$) CDW's that have $\phi = n \times 30^\circ$ where n odd possess contour patterns of like shape. For the commensurate state shown, a CDW of this odd- n type appears seated in a symmetric fashion on the predefined $3a_0$ supercell. Label a is here kept for the cation which (effectively) marks the crystallographic origin in the superlattice as established, this identification being made in the symmetry approved manner (Ref. 3). Relative to this crystallographic unit, we see location A in the CDW to take a displacement equivalent to 120° , falling at the crystallographic B site (here cation b). This situation is now compatible with a relabelling of the CDW phase angle relative to the crystallographic origin as 210° , since in this ϕ still is manifest as being $n \times 30^\circ$ with n odd.

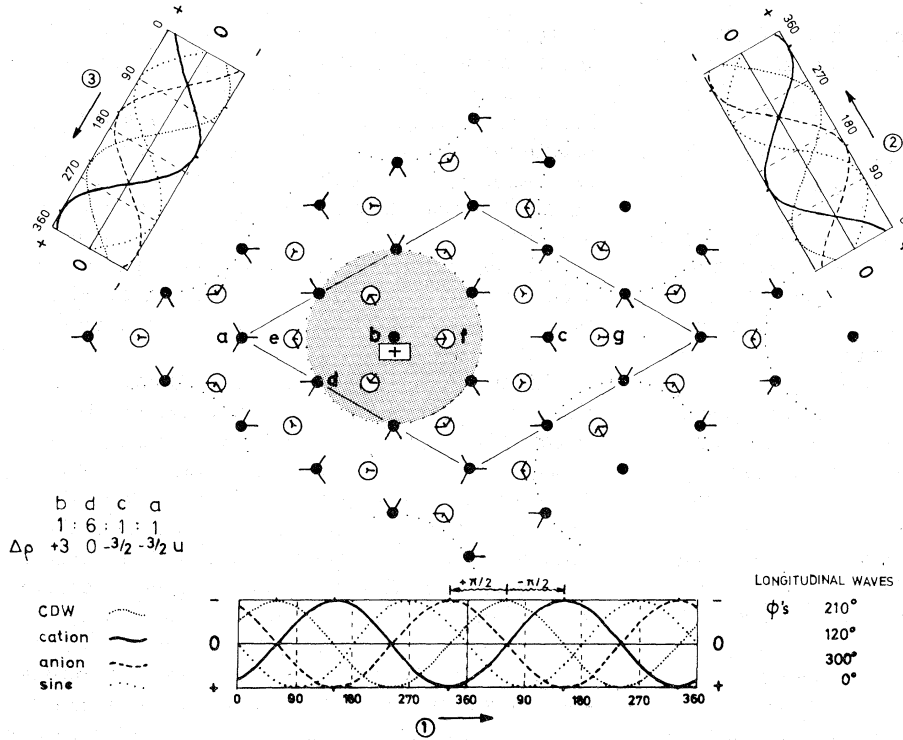


FIG. 5. Idealized counterpart of Fig. 3, showing anion and cation waves in quadrature with $\phi = 210^\circ$ CDW: i.e., $\phi^A = 300^\circ$, $\phi^C = 120^\circ$. Displacement details are given in Table III. Shading indicates region with deficit of negative charge.

$$\begin{matrix} b & d & c & a \\ 1 & 6 & 1 & 1 \\ \Delta\rho & +3 & 0 & -3/2 & -3/2 & u \end{matrix}$$

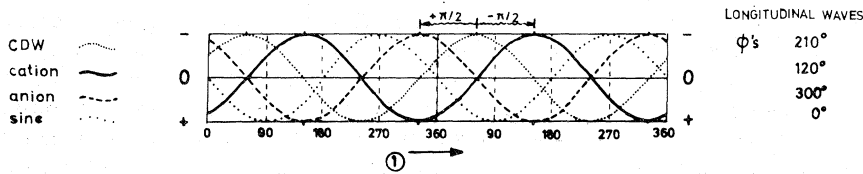


TABLE III. Upper-sandwich basal-plane displacements under "idealized" phase conditions for a $\phi = 210^\circ 3a_0$ commensurate CDW: namely, with cation wave showing 90° lag (i.e., $\phi = 120^\circ$) and anion wave in antiphase (i.e., $\phi = 300^\circ$) (see Fig. 5).

Atom label	Component displacement pattern at atom	Resultant as fraction of single wave amp. ^a
where		
Ta	a	$m = C \sin(120) = C \sin(60)$
	b	$n = C \sin(120 + 240) = C \sin(0)$
	c	$o = C \sin(120 + 480) = C \sin(60)$
	d	[Resultant turned 30° from $(11\bar{2}0)$]
where		
Se	e	$p = A \sin(300 + 80) = A \sin(20)$
	f	$q = A \sin(300 + 320) = A \sin(80)$
	g	$r = A \sin(300 + 540) = A \sin(40)$

^aThe equivalent values for Fig. 6 are $-1.50C$, $+1.71A$, $-1.44A$, and $-1.03A$, all in $(11\bar{2}0)$.

value being strongly peaked at $-(+)$ 1. For n even, the corresponding values are $+(-)$ 2.866, $-(+)$ 2.866, and 0. The asymmetric form taken by the NMR data (see Figs. 1 and 3 of Ref. 5) clearly marks the actual situation as being very much closer to an odd- n -type case. $\Delta\rho_{\max}$ is plus 3 units for $n=3, 7,$ and 11 . By our examination of the commensurate periodic-structural distortions (CPSD) in $2H$ -TaSe₂ we have seen the charge modulation map becomes suitably placed relative to the crystal structure following the choice $n=7$.

Unlike the situation with $1T$ -TaSe₂ (where the various effects of the CDW are up to an order of magnitude more pronounced than in $2H$ -TaSe₂) it is not possible in $2H$ -TaSe₂ to achieve x-ray photoemission from the Ta $4f$ levels at a resolution sufficient to separate the various cation sites, and thereby gain further independent information on the CDW phasing⁶ (see Sec. IV D). The NMR relaxation data⁵ from $2H$ -NbSe₂ substantiate that less than 10% of the Fermi surface is gapped by the CDW, and interpretation of the de Haas-van Alphen (dHvA) data from $2H$ -TaSe₂ indicates⁷ that the situation is little more pronounced there. In the $1T$ case, by contrast, at least three-quarters of the Fermi surface is gapped by the CDW.¹² The charge modulation amplitude reaches about a full electronic charge,⁸ as compared with certainly less than $\frac{1}{2}e$ in the $2H$ case,^{5,9} and the maximum atomic displacements reach about 8% of a_0 ,¹⁰ compared with only 2% (Table II) in $2H$ -TaSe₂.

We now turn to consider question (b) raised at the start of Sec. III. The cations, it would appear, might pick up their dominant shifts in the superlattice state on two counts. (Note in the two-dimensional Fig. 4 that cations d and anions f sit at points of approximately the same apparent potential gradient from the CDW.) First, the anion sublattice is quite tightly packed, whilst at the same time the cation is rather small for its coordination cage. Such structures are (for transition metal cations) often open to a certain amount of specific intercation d -electron pair bonding (cf. d^1 NbO₂, NbI₄, and NbS₃).¹¹ Nonetheless, in the present case the author feels that any such cation pairing to be inferred from the displacement pattern of Fig. 2 is of secondary importance. The intercation distance in the apparent pairings there has been reduced (at 5 K) by only 4%, compared with² 13½% in NbI₄ or 9% in VO₂, and with 20% in the chains of d^2 WTe₂. Moreover, the structure of Fig. 2, when viewed simply as a vehicle for d^1 cation pairing, is not as efficient, even within the present hexagonal limitations, as are the $\sqrt{7}$ (2 by 1), or $\sqrt{13}$ cells (3 by 1). This is not to say though [it being taken that the closely $3a_0$ periodicity follows from a $\chi^0(q)$ determined instability under the

given Fermi-surface geometry¹²] that the phase of the resulting CDW is not through incipient pair-bonding encouraged further to favor $\phi = 210^\circ$, and the situation of Fig. 5, over say $\phi = 240^\circ$, and the situation of Fig. 6.

At this point we are brought to the second significant factor effecting the dominant modulation of the cation sublattice. This lies in the prevailing electronic circumstances which surround the CDW itself. The open band that supports the modulations of the CDW is high in d_{z^2} character. In view of the present largely tight-binding situation, these charge modulations will be confined to the vicinity of the central cation-bearing sheet in the MX_2 sandwiches. It follows that the forces within this sheet will be the greater, especially in view of the small wavelength for the present CDW, and of the short screening length within a metal.

The observed deviation from antiphase between anion and cation waves, and their phasing shifts from quadrature with respect to the $\phi = 210^\circ$ CDW, appear largely an outcome of steric and bonding effects that are encountered under the motions attempted. Chemical binding energy is largely held in the bonding s and p bands and set by the least anion-cation separation. Hence, when a structure distorts, these M - X "bonds," though open to a fair degree of rotation, are much less open to longitudinal change. (For example in the distorted phase of VO₂, although there is a 9% reduction in the V-V separation in the c -axis pairs, there occurs a concomitant limiting change in V-O separation of only 5%, Ref. 11, p. 288.)

Let us consider first the motion of selenium atom g in Fig. 5 (the ideal case). The general antiphase character of its resultant motion carries it towards a pair of flanking cations (d) which are coming together into its path. If we compare this situation with the observed one presented in Fig. 3, we see that the strong motion of these cations actually is sufficient to reverse the resultant displacement acquired by anion g (with just a small forward component being communicated to the cations). At the same time a phase change of this form imposed on the anion sublattice PSD will have the effect on anion f of reversing its sense of motion too. This helps here to prevent M - X bonds from being overextended by the retreat of cations d . The remaining type of anion e will continue to receive a forward resultant much as in the antiphase situation. This is quite appropriate as there the cations are moving transversely to the M - X bonds. The net effect on the PSD phasing of this interaction between the sublattices under the motions attempted is a change in the cation phase from its ideal value of only $+14.2^\circ$, whilst the anion wave suffers a shift of $+80.6^\circ$. The latter

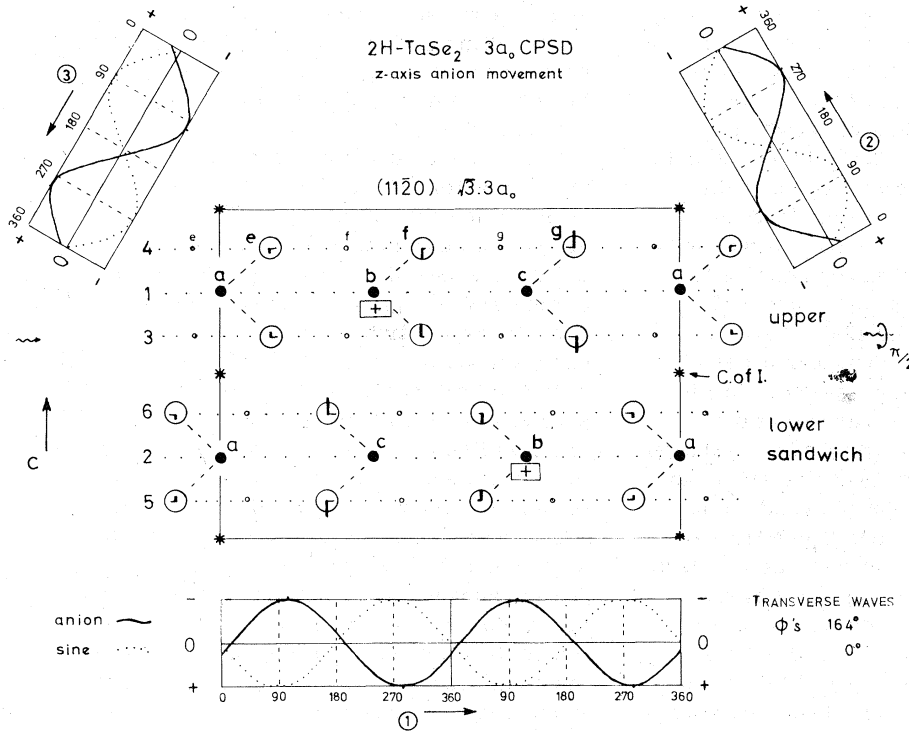


FIG. 7. c -axis anion displacement wave [$\phi^A(\parallel \bar{c}) = 164^\circ$] for 2H-TaSe₂ 3a₀ commensurate CDW. The three waves are projected into a (11 $\bar{2}$ 0) slice (contains all three anions e, f, g and their displacements), at the level of atom 3 in Fig. 1. The "ride up" of anions g about cations c in the upper sandwich seats into the "hollow" created about cation b by anions f in the lower sandwich (and vice versa).

displacement wave is brought then almost to anti-phase with the starting CDW.

Primary bonding considerations similar to those above seem to be preeminent too in determining the independent phasing of the accompanying c -axis polarized component to the anion motion (Table I). In the above motions, as anions g are pushed back onto stationary cation c with its negative charge excess, they ride up into the Van der Waals gap. Concurrently, anions f , as they are pulled away in the basal plane from stationary cation b , have to swing in towards the sandwich center. Likewise anions e are pulled in somewhat with the recession of cations d . These c -axis motions are presented in Fig. 7, which is based on the data^{1b} of Table I. We note in the latter that the c -axis amplitude of the anion waves is twice that exhibited in the basal plane. This is a reflection of the absence of strong bonding forces emanating from the intersandwich regions. The observed c -axis phasing lies within 4° of giving a resultant maximum outward displacement over cation c , sited at the negative maximum of the CDW. This swelling in the upper sandwich comes to sit quite happily into the depression around cation b within the "inverted" lower sandwich of the 2H stack, and so does not force the sandwiches apart.

We can now add one or two further comments in response to question (c) raised at the start of this section. Although for a commensurate CDW-PSD

ϕ may be assigned one or other of the 12 symmetric $n \times 30^\circ$ values, there are in fact here only three physically distinct (high-symmetry) charge situations being offered to the system. The various ϕ labels subsequently state how the system has responded, and where the crystallographic origin arises relative to the CDW phase origin (see caption to Fig. 4). Physically the even- n CDW, being symmetric in plus and minus $\Delta\rho$, offers only one distinct situation, while by contrast the odd- n offers two ($+3, -\frac{3}{2}; -3, +\frac{3}{2}$). The second odd- n -type shortly will be encountered in the octahedrally coordinated 1T materials. It automatically clusters the cations towards the center of the negative charge regions. For the 3a₀ supercell the six atom clusters around the cell corners to be seen in Fig. 38(a), of Ref. 2 correspond to $\phi = 270^\circ$, but it is a situation that is not favorable to a screw hexad with 2c₀ stack.

IV. CHANGES IN THE PSD UNDER PRESSURE AND TEMPERATURE

We open this section with some comments on the effect of pressure on the 2H CDWs. With regard to the phase angles, it has not been determined how they might alter under pressure. However, since the soft element in the structure is the Van der Waals gap, and seeing that the sandwiches seat together quite well initially, it is probable

that to begin with relatively little change is wrought in these angles.

What pressure has been observed to cause are small changes in the incommensurate CDW onset temperature (~ 0.3 °K/kbar).¹³ Since the changes (i.e., of T_0) can be either positive ($2H$ -TaSe₂) or negative ($2H$ -TaS₂ and $2H$ -NbSe₂), they probably result from small changes in Fermi surface (particularly in the sensitive and important ΓK direction)⁷ that, respectively, strengthen and weaken the size of the active peak in $\chi''(q)$. What associated changes under pressure might occur in the *on-set* value of the CDW wave vector are not yet known: nor are they calculable with any certainty.¹² Upon cooling, the rapid reduction towards a commensurate value of $\frac{1}{3}a_0^*$ observed in the condensed wave vector, has in fact been shown in Ref. 1(b) to derive not from a band-structure effect, but from the coupling in of a secondary distortion of wave vector $g - 2q_0$. Such admixture increases rapidly as the primary amplitude grows upon cooling. Its presence in the ICDW phase works against a simple analysis of the commensurate transition also. At this stage it is probably a mistake to attribute the quite strong depression in the lock-in temperature T_d observed in $2H$ -TaSe₂ under pressure (2.7 °K/kbar),¹³ to growth in the deviation from commensurateness during the above-noted elevation of T_0 . [The reader is reminded here that q_0 is only 2½% short of $\frac{1}{3}a_0^*$ at T_0 in $2H$ -TaSe₂ and NbSe₂,¹ while 4% greater than $\frac{1}{3}a_0^*$ in $4Hb$ -TaSe₂ (Ref. 14) right down at 10 °K.]

Upon lock-in, we clearly may encounter significantly changed physical phenomena. Thus, only after the superlattice period is established may the CDW-modified Fermi surface be folded back into a reduced Brillouin zone, there to define small fixed extremal superstate orbits. A comparison of the dHvA data for commensurate $2H$ -TaSe₂ versus incommensurate $2H$ -NbSe₂ shows this directly (see Ref. 7). In terms of energy nonetheless, it is found that the ultimate lock-in transition itself can be a very slight event. ΔH at T_d in $2H$ -TaSe₂ is probably only ~ 0.05 cal/mole.¹⁵ McMillan¹⁶ has indicated how much of the commensuration energy may already come out of the CDW system prior to ultimate lock-in, through the formation of "discommensurations." These should form in regular array (much as a dislocation net), and are narrow regions of gross phase modulation, segregating out to leave wide regions over which the CDW is thereby rendered commensurate. Indirect evidence for this phenomenon in the $2H$ materials is found in the high and strongly frequency-dependent internal friction at T_d , revealed earlier in Young's modulus measurements.¹⁷ Raman measurements⁴ also indicate now, in one's ability to

follow peaks up through T_d , that the superlattice selection rules established for the commensurate PSD are not sharply modified by passage into the "incommensurate" phase. Unfortunately, high-resolution Raman results are not yet available for $2H$ -NbSe₂ in its low-temperature ICDW phase. However, the well-peaked character of the previously mentioned NMR data for this material⁵ below T_0 does support the above conclusion.

Raman measurements were actually reported some time ago on $2H$ -NbSe₂ up above T_0 at liquid-nitrogen temperature,^{18(a)} and these now highlight a new feature of interest. A comparison of the second-order (two-phonon) peaks with those given by semiconducting $2H$ -MoS₂ reveals^{18(b)} for $2H$ -NbSe₂ an unusual, broadly peaked, and very intense band of absorption covering the range 130–230 cm⁻¹. This same feature recurs in $2H$ -TaSe₂ ($T > T_0$) from 90 to 160 cm⁻¹.⁴ The peak values here, of 180 and 135 cm⁻¹, respectively, are just twice those at which the longitudinal acoustic branch levels off in ΓM beyond $0.2a_0^*$ [see Fig. 8(b)]. Clearly this branch, so strongly affected by the developing singularity in $\chi(q)$, picks up an abnormally large polarizability. A continued high polarizability subsequently is apparent, once below T_0/T_d , in the high *first-order* Raman intensities of those superlattice lines to be generated from this particular branch. [Below T_0/T_d , (for all branches, of course) the six points of the star $\frac{2}{3}\Gamma M$ become folded into Γ , along, incidently, with two K points.] Such high intensity is not found to derive from the other acoustical branches, (even though these are somewhat softer than might be expected¹⁹). Surprisingly, this seems so for the optical branches as well, and in particular for the longitudinal Σ_1 branches out of Γ_5^+/Γ_6^- (E_{2g}/E_{1u}). Unfortunately, these optical branches have yet to be traced out by neutron scattering techniques for a group-V dichalcogenide, but Fig. 8(a) gives their general form and structure in the directly related d^2 semiconductor $2H$ -MoS₂. Figure 8(b), in which we have incorporated the zone-center Raman data, makes it apparent that for the d^1 case of $2H$ -TaSe₂ appreciable interaction between the acoustical and the lower optical modes is plainly conceivable.

Earlier, when discussing the commensurate condensed state we examined the phase relationship between the two sublattice waves of the PSD; the product of a basically LO condensation and its accommodation to the strong bonding forces in the underlying lattice. Apparently, that phase relation becomes little altered upon moving to the case of $2H$ -NbSe₂,¹ a result again more indicative of a discommensurate than an incommensurate condition. However, within the "normal" phase, well above T_0 , one must encounter a more radically

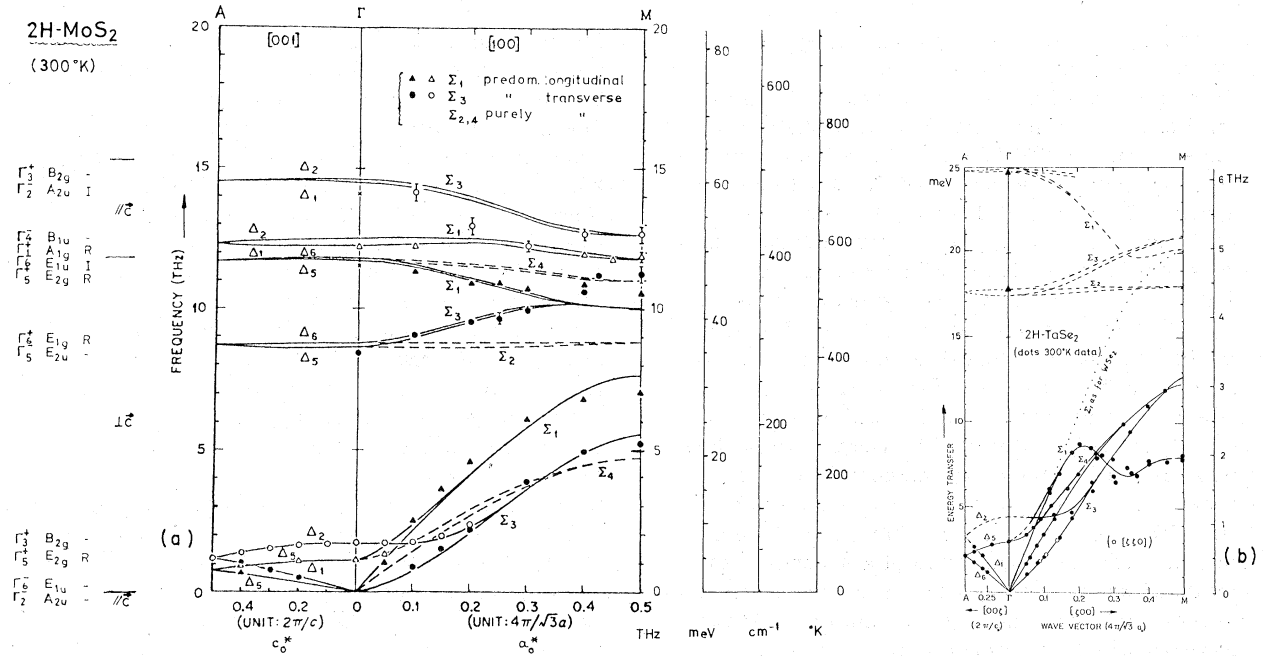


FIG. 8. Phonon dispersion curves in $2H\text{-MoS}_2$ and $2H\text{-TaSe}_2$ (a) Room-temperature curves for $2Hb\text{-MoS}_2$, including Γ point symmetry and optic information. The solid and dashed lines are as calculated by a force field model; the dots are the experimental data [Ref. 19(b)]. (b) Room-temperature curves for $2Ha\text{-TaSe}_2$. The longitudinal acoustical branch is doubly degenerate by q_0 . The solid lines are here guide lines through the experimental points (Ref. 1). The dashed lines are estimates made in the light of the optical data (Ref. 4) and Fig. 8(a).

changed situation. The phonons around q_0 which are being affected by the developing singularity in $\chi(q)$, are not yet phase related in the three axial directions, not as yet being mutually phase anchored to each other, let alone the lattice. The displacement pattern of Fig. 3 is the outcome proper to the selected phasing of the CDW, to its symmetry and to its geometry relative to the lattice. These characteristics will not be met by the uncoupled phonons well away from T_0 . The Kohn anomaly, evident in the acoustical phonon dispersion results¹ at 300 °K (i.e., greater than $2\frac{1}{2}T_0$), is therefore not simply and directly to be connected through into the actual low-temperature long-range condensation. In fact, we know that the longitudinal acoustical branch with its strong Kohn anomaly, though depressed over a wide range of q , never is carried sharply to zero at q_0 at T_0 , despite $\chi^0(q)$ being quite well peaked there.¹²

Since the singularity being promoted has a wavelength as short as $3a_0$, even a simple condensing acoustical mode would in fact bring into a parent unit cell the substantial optical offset of 80° between *actual* displacements at the anion and cation sites there. Conversely, optical character to cell-site displacements under a simple optical mode condensation would be lessened by the same

amount. For the experimental condensed situation (where $\Delta\phi$ between the sublattices is not tied to 0 or π) examination of Fig. 3 when made *on a cell-site basis* shows it to be of quite variable local character. The scant (and currently indirect) evidence for any strong Kohn anomaly occurring too in the optical branches is now simply accounted for. The softening, as for the acoustical branches, is partial only. Moreover, should we consider a frequency renormalization equation of the form²⁰ $\omega^2 = \omega_0^2(1 - g^2/\omega_0)$ [i.e., $(1/\delta^2)\omega_0(2\delta - g^2) = 1$ where $\delta = \omega_0 - \omega$], then for a set mode depression δ the electron-phonon coupling strengths g would have to rise as ω_0 rises and the amplitude of the phonons falls.

V. COMMENTS ON THE PSD'S IN RELATED MATERIALS

A. TiSe_2

The $2a_0 \times 2a_0 \times 2c_0$ CDW-PSD which condenses in TiSe_2 below 200 °K casts further light on the selection of long-range super-order in this class of layer materials. In d^0 TiSe_2 this state occurs under electron-hole coupling in the semimetallic situation of small indirect p - d , ΓL overlap.^{21,22}

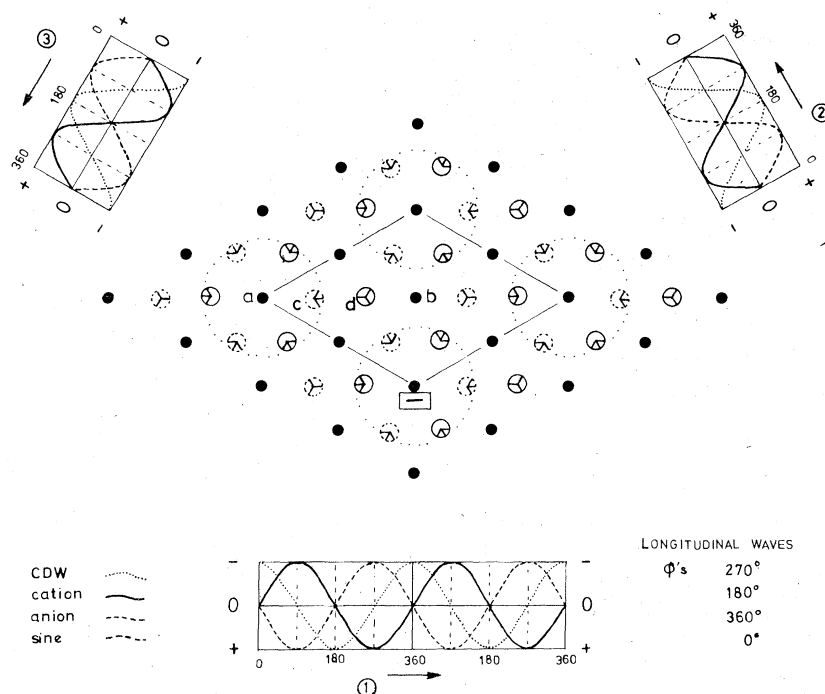


FIG. 9. Displacements for a $2a_0$ triple-axis PSD in the CdI_2 structure, with ideal longitudinal motions accompanying a $\phi = 270^\circ$ CDW; i.e., $\phi^A = 360^\circ$, $\phi^C = 180^\circ$. Displacements in the two anion sheets would be equivalent; the cations are undisplaced. Note anions sometimes are locally shifted longitudinally to an $M-X$ bond, sometimes transversely. This distortion pattern is not that shown by TiSe_2 .

As in almost every case for the layer compounds, the system undergoes a symmetric triple-axis condensation. In TiSe_2 the space group passes from $P\bar{3}m1$ to $P\bar{3}c1$. However, since we deal here with trigonal rather than hexagonal symmetry, and in particular with octahedral rather than trigonal prismatic local coordination, the choice of phasing is more restricted than for the $2H$ materials earlier. In fact, were it bound to strict optical phasing in *longitudinal* polarization, it becomes limited to $\phi^A = 360^\circ$, $\phi^C = 180^\circ$, if one is to see preserved physical equality between the two anion sheets per sandwich (see Fig. 9, each cation forms a center of inversion for its coordinating anions). With this choice (given the $2a_0$ wavelength), only the anions would move (as to a CDW with phase 270°). From what has gone before, this is seen not to be encouraging to realization of the condensation in this form. Moreover, the charge and displacement pattern is not compatible with the $2c_0$ stacking that the Fermi surface geometry is calling for.

In $2H\text{-TaSe}_2$ the $2c_0$ supercell was observed to maintain a center of inversion in the Van der Waals gap (rather than in the sandwich) and likewise the $2a_0$, $2c_0$ PSD actually developed by TiSe_2 does indeed retain a CdI_2 structure gap center of inversion, whilst relinquishing those in the sandwiches. This PSD²³ forsakes longitudinal for transverse waves, though one does see retained a strong locally antiphase character under phasing $\phi^A = 90^\circ$,

$\phi^C = 270^\circ$. This phase choice is what is now required for preservation of anion sheet equivalence within a sandwich. In the lower sandwich, the phases convert to $\phi^A = 270^\circ$, $\phi^C = 90^\circ$. (As previously, this phase labeling is made relative to the symmetry standardized³ crystallographic origin of the superlattice.)

In this observed transverse wave situation, three-quarters of the cations are displaced. These cation displacements, and likewise those of the anions, are not now of course of the type with which we became familiar in Figs. 5 and 6. No longer can there be any simple idealized quadrature relation to the associated CDW. Physically, the low-temperature superorder presented in Fig. 10 is envisaged to arise as a cooperative coupled condensation of holes and electrons onto the crystal lattice. In the prevailing tight-binding situation, the holes are closely associated with the selenium sublattice, the electrons with the titanium. The atomic motions under the condensing mode are such as to see three-fourths of the atoms present brought into loose TiSe_2 clusters, this effective anion-cation attraction being met by the optical phasing to sublattice motions. The form of the displacement pattern is rather like an antiferroelectric. However, the driving force for the state comes from the special form of the band structure and $\chi^0(q)$, in the semimetallic situation just engaged by TiSe_2 .^{21,22} Neither the degenerate semiconductor TiS_2 , nor highly semimetallic TiTe_2 ,

lower amplitude PSD.

According to the present model the atom-type groupings are

	Total/Sandwich	Atom Type					
		<i>a</i>	<i>b</i>	<i>c</i>	<i>d</i>	<i>e</i>	<i>f</i>
<i>M</i>	16	1	6	3	6		
						<i>g</i>	<i>h</i>
<i>X</i>	32	6	6	2	6	12	

In constructing Fig. 11 we have employed longitudinal modes with the "ideal" antiphase $\phi^A = 360^\circ$, $\phi^C = 180^\circ$, best suited to preserve equivalence between the two anion sheets per sandwich. This, as in $1T$ -TaS₂ (Sec. VD) and TiSe₂ (Sec. VA), seems a most desirable feature, for it inhibits a *c*-axis displacement components being conferred on the cations. Such symmetry across the cation plane is most appropriate in view of the d_{z^2} origins of the CDW-PSD in these d^1 - d^0 materials. It is not a universal feature to distortions of the CdI₂ structure (witness $d^4 \sqrt{3} a_0$ PtBi₂). The CDW associated with the above sublattice waves takes the phase $\phi = 270^\circ$. Once again, as with $2H$ -TaSe₂, we are led to an odd-*n* CDW. The $\bar{3}$ symmetry center is now, however, sited at the supercell corner. A phase shift of π introduced in all the waves would produce the same symmetry, but the re-

versed sign of the displacements leads to a displacement pattern that is less attractive, as shortly we shall witness for $1T$ -TaSe₂ and TaTe₂. Experience however with the "simpler" cases of $2H$ -TaSe₂ and TiSe₂ should prepare one not to be too surprised by added complexities in the ultimate realization of this condensation in VSe₂.

C. NbTe₂ and TaTe₂

In the $4d^1$ and $5d^1$ $1T$ materials, it is assumed the observed CDW-PSD effects are stronger because the "bare" phonons are initially of lower energy, and the electron-phonon coupling is larger. Certainly the nonrelativistic band structures themselves are not substantially different than for $3d^1$ VSe₂.²⁶ (Moreover, relativistic modifications of the lower d_{z^2} dominated sub-band of the t_{2g} set are expected to be small.) The strongest CDW effects are found accordingly for the heavier tellurides (see Ref. 2, Sec. 5.2f). Indeed the effects there are sufficiently different from the sulphides and selenides for these tellurides to have to be treated separately.

Normally, as discussed in Ref. 2, the distortion present in NbTe₂ and TaTe₂ suggests the action of a single-axis CDW of wavelength $(\sqrt{3}/2) \times 3a_0$, running in the ΓM direction. More recently, it has been found³⁰ that pulse heating in the electron beam locally can revert the material to a seem-

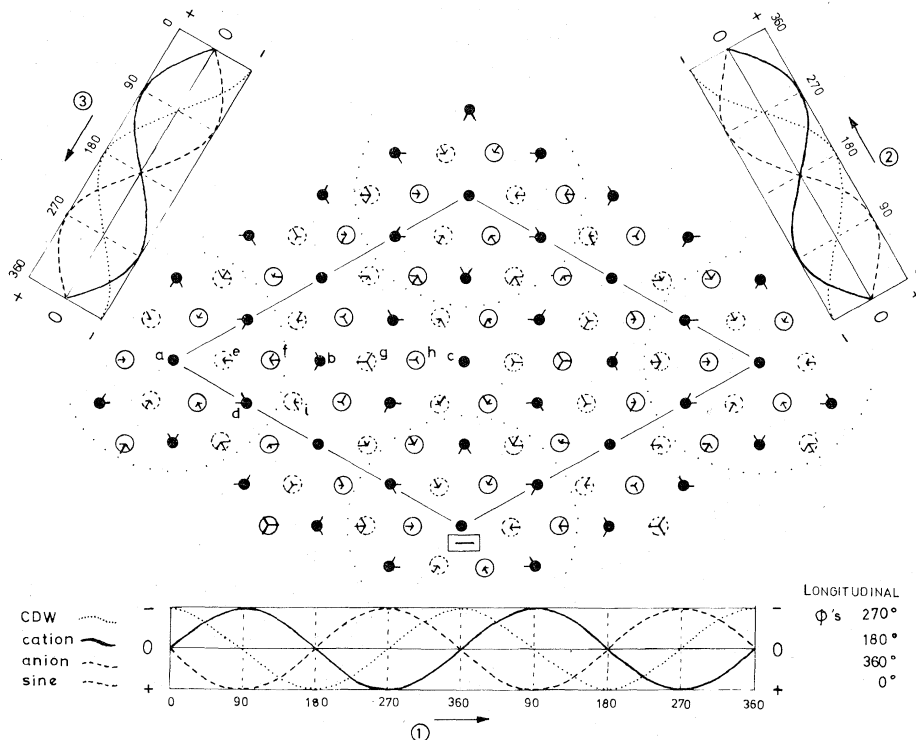


FIG. 11. Idealized $4a_0$ triple-axis longitudinal PSD relevant to VSe₂ low-temperature phase. The anion phasing, $\phi^A = 180^\circ$, with the cations in ideal antiphase ($\phi^C = 360^\circ$), is chosen to make the two anion sheets per sandwich equivalent. The accompanying CDW again then takes an "odd-*n*" phasing, $\phi = 90^\circ$. Shifting the phasing by 180° would destroy the formation of the 13-atom cation stars around the cell corners.

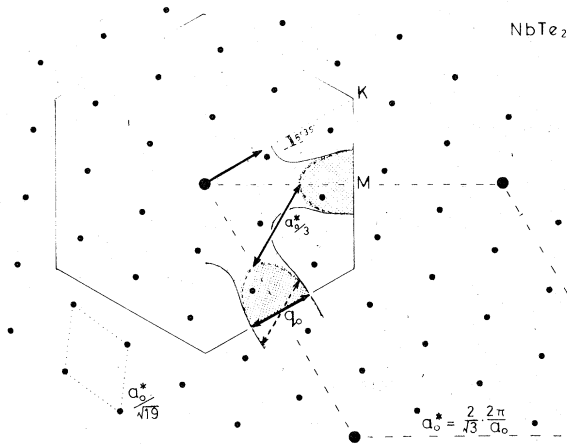


FIG. 12. Relation of the observed single- and triple-axis PSD's in NbTe_2 or TaTe_2 to a Fermi surface extrapolated from the calculated results for the $1T$ sulphides and selenides. The dish about the Γ point has become much expanded. The triple-axis PSD is again associated with "spanning" across the M point, but parallel to ΓK , not ΓM . The $\sqrt{19}a_0$ commensurate PSD is reached by a $6^\circ 35'$ rotation. The superlattice diffraction spots are shown. The single-axis PSD comes from saddle-point nesting with $\vec{q}_{0s} = \frac{1}{3}\vec{a}_0^*$. (N.B., $q_{0s} = 2\pi/a_m/2$.)

ingly unrelated triple-axis state, commensurate at room temperature, but readily rendered incommensurate just above. The commensurate condition here is a $\sqrt{19}a_0$ "3-by-2" rotated hexagonal cell. The incommensurate condition yields diffraction patterns which show that the rotation actually involved here is one of $6^\circ 35'$ from ΓK (i.e., from \vec{a}_0), and not of $23^\circ 25'$ from ΓM (as might have been suspected from earlier experience with the $1T$ sulphides and selenides). We display the relationship between the two diffraction patterns and the parent Brillouin zone in Fig. 12. This figure should be compared with Fig. 34 in Ref. 2 for $1T$ - TaSe_2 , etc. It appears that the incommensurate wave vectors are once again to be associated with Fermi surface nesting "across" the M points, as in the other $1T$ group-V materials. Now, though, the ΓK orientation of the incommensurate vectors shows that it no longer is profitable to overall nesting for the triple-axis CDW to take on a 30° rotation in the basal plane (see Ref. 2, Fig. 32). Moreover, it is further found³⁰ that the q_{0i} 's do not tilt out of the basal plane, unlike for either VSe_2 or $1T$ - TaSe_2 (see Ref. 26, Figs. 11 and 12).

Normally, as mentioned, NbTe_2 and TaTe_2 do not occur with the above triple-axis CDW-PSD, but with a single-axis state. The form of that PSD was given in Ref. 2, Fig. 35, and Ref. 31, Fig. 4. The effective wavelength is $3 \times (\sqrt{3}/2)a_0$, with the

wave vector parallel to ΓM ; i.e., $\vec{q} = \frac{1}{3}\vec{a}_0^*$. As can be seen in Fig. 12, this is too large even to represent diagonal nesting "across" M . On that figure a suggested source for coupling of this periodicity is indicated. The form of Fermi surface being advanced here falls in reasonable progression from the $5d^1$ sulphides and selenides. The dish at Γ , which depends on the t_{2g} -band crossover within ΓA , and also on the lowering in energy (for this band) at Γ of the Γ_1^+ (d_{22}) eigenvalue relative to Γ_3^+ ($d_{xy}, d_{x^2-y^2}$),²⁶ is shown made more developed than in the selenides. In the terminology of the latter reference, the double muffin-tin discontinuity is smaller in the telluride, and so its counteraction of the trigonal distortion becomes less (Ref. 26, Table 4). [The trigonal distortion remains approximately the same in VSe_2 , $1T$ - TaSe_2 , and NbTe_2 , ($c/a \approx 1.8$).]

The detailed behavior of the single-axis charge-density wave as a function of temperature is not simple, and has not been fully explored with good quality material. Figure 78(e) in Ref. 11 gives a typical room-temperature diffraction pattern. This is shown indexed in Fig. 13, following Ref. 30. The arcs of diffuse scattering evident in the above-quoted plate have been included. It is possible that this scattering comes from c -axis disordering of the corrugated monoclinic stack by nonstoichiometric defects (see Fig. 4, Ref. 11).

We note by contrast, at this point, that no diffuse scattering arcs were seen in the alternative triple-axis condition prior to rotational lock-in. This likewise is in contrast with the triple-axis situation for $1T$ - TaSe_2 . Since such scattering con-

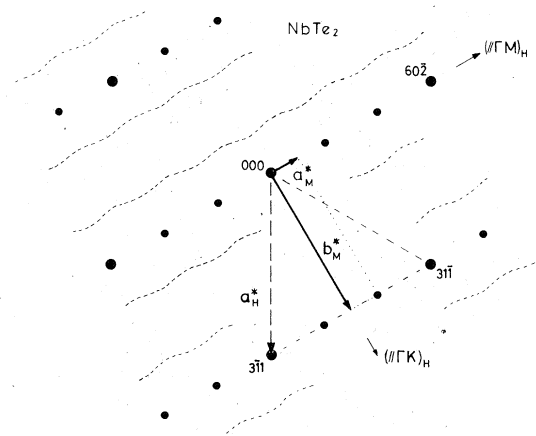


FIG. 13. Reciprocal space for single-axis NbTe_2 . The diffuse scattering takes the form of corrugated sheets flanking each close-spaced row of superlattice spots; at approximately $\frac{2}{7}$ of b_m^* from these. a_m^* appears to become incommensurate as the temperature is raised (in place of $\frac{1}{6}a_0^*$).

atively on a simple local chemical valence bond model. The single-axis case of NbTe_2 had long since been noted not to be assignable to this category. The extensive MnP family presents a further case. In the latter case a chain-type distortion of the regular hexagonal NiAs structure occurs over a wide range of electron contents (e.g., d^2 VAs, d^3 VS; d^4 MnP, d^5 FeP, d^6 CoP). The distortion also arises in triple-axis form in low-temperature NbS. As demonstrated in Ref. 34, the MnP-type distortion evolves under a rather general form of attractive intercation potential. [Additional witness to a general tendency towards distortion for the NiAs structure is borne by FeS (troillite), NiS (millerite), and NiP].³⁵ It is accordingly unreasonable that the distortion observed³⁶ in VS should alone be taken as coming from the action of a Fermi surface governed instability.

Haas, following the above work on MnP,³⁴ and in the light of the crystallographic results of Ref. 10 on commensurate $1T$ -TaS₂, has indicated that the 13-atom star found in the $1T$ structure likewise might possess a rather general intercation-based stability with regard to the CdI₂ structure. Inspection of the upper region of Fig. 14 (where the measured cation displacements of Ref. 10 are given, and the odd- n -type CDW of Ref. 2, Fig. 31a superposed), immediately will reveal that the displacements are not sinusoidal. The displacement of cation c is larger than that of cation b , despite it being at a point of lower (apparent) potential gradient. The star is contracted as a unit, the inner ring of six atoms carrying the outer ring of six atoms in with it. We still have the symmetry-determined 6:6:1 cation ratio, already indicated in the XPS,⁸ Mössbauer³⁷ and time-dependent-perturbed-angular-correlation³⁸ data, but the relationship between the three sites is strongly perturbed from the simple sinusoidal model, and numerical analysis should not be carried too far at this stage. It is evident that the size of the displacements, not to mention the size of the cation muffin tins are not at all insignificant in relation to CDW wavelength. Clearly then a point-cation infinitesimal-displacement model has to be heavily qualified through harmonics. These have been noted to play a significant role even for the $2H$ ICDW's.¹ More recently, they have been shown to be very active in the unusual "quasicomensurate" state of $1T$ -TaS₂.⁴⁰ The continuity problems presented then in the $1T$ case are, it is evident, even more awkward than for the $2H$ case discussed earlier.

If above, supplementary to the CDW effects, we might indeed be involved with an incipient pair bonding or a general stability in the strongly demarcated 13-atom star of $1T$ -TaS₂, its recurrence ought to be watched for in the commensurate $\sqrt{19}a_0$

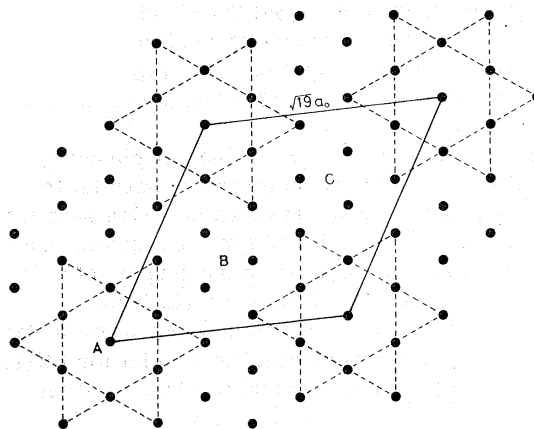


FIG. 15. The 13-atom stars in $\sqrt{19}a_0$ superlattice; six of the 19 atoms per cell are now outside these stars.

phase of NbTe_2 (see Fig. 15), or indeed in $4a_0$ VSe₂ (see Fig. 11), as these structures come to be refined.

Let us now turn to a closer inspection of Fig. 14. Following our line of interpretation for the earlier cases, we see that, within a CDW-based model, the cell-cornering cations must locate the points of maximum negative charge surfeit. These atoms are then those most strongly driven towards the valence state $\text{Ta}^{3+}(d^2)$. This conclusion runs directly counter to recent interpretation of both XPS (Refs. 6 and 8) and Mössbauer (Ref. 37) results, which would see an approximately d^0 Ta^{5+} atom at site a . Since it is known, from the evidence borne by the q_0 variable incommensurate phase in mixed d^1 - d^0 (Ta, Ti)S₂, that the dimensions of the Fermi surface play a crucial role in determining the present PSD geometry,² it is felt one must seek a release from that interpretation, and not at this stage be tempted to pass over to emphasis of a chemical binding model. We would allot only a secondary role to such effects, as testified to by the limited vigor with which the system clings to a $\sqrt{13}a_0$ commensurate state under isoelectronic doping.³³ One is left then with the task of reinterpreting the XPS and Mössbauer data in a manner compatible with the now revealed form of the PSD in $1T$ -TaS₂ and its previously ascribed origin. As stated above, this calls for reversing the sign of the CDW from its currently advanced direction, through a shift of π in phasing.

To minimize confusion at this point, let it be noted that the CDW phase angle associated with Fig. 14 is 270° . Misleadingly in Ref. 2, Fig. 33, we set upon much the same displacement pattern a phase angle $\phi = 90^\circ$, following our usage there, in Fig. 31, of the leading positive sign to denote

excess *electronic* charge. (There also we gave the site types different labels from those now chosen). In our present usage $\phi = 90^\circ$ is, of course, precisely the phasing designed to make the unique cell concerning site *a* positive; the very selection that, as we see, we now are to avoid.

Since the interpretation given to the Mössbauer data is strongly colored by that already given to the XPS data, we will examine the latter first. In Fig. 16 we display the contrasting valence situations at the cation *a*, *b*, and *c* sites for the $\phi = 90^\circ$ and $\phi = 270^\circ$ CDW's, under the simple sinusoidal assumption of Fig. 31a, Ref. 2, and taking $\delta\rho$ at the *a* site to be exactly one electron. The substantial splitting of the Ta 4*f* lines which is found in the XPS spectra indicates that the latter assumption is not too excessive. It here might be noted that the $\phi = 270^\circ$ case probably is to be favored chemically over the $\phi = 90^\circ$ case, for it swings the six *c* site cations towards the more acceptable 5+ limit. In Fig. 16 we have oriented the charge scale so that it corresponds to the conventional presentation of XPS data, where binding energy is shown increasing towards the left. We then read the $\phi = 270^\circ$ situation as 6:6:1, the $\phi = 90^\circ$ as 1:6:6. Relative to the two strong peaks, arising from sites *b* and *c*, a corresponding peak free from any CDW shift would lie closer to the left-hand peak in the $\phi = 90^\circ$ case, but closer to the right-hand peak for $\phi = 270^\circ$. The spectra of Ref. 8, Fig. 4, which follow the peaks under increasing *T*, do indeed appear to support the latter choice. This also is the case with Fig. 8 of Ref. 6, which shows emission from 2*H*-TaSe₂ as a function of temperature alongside that from 1*T*-TaSe₂.

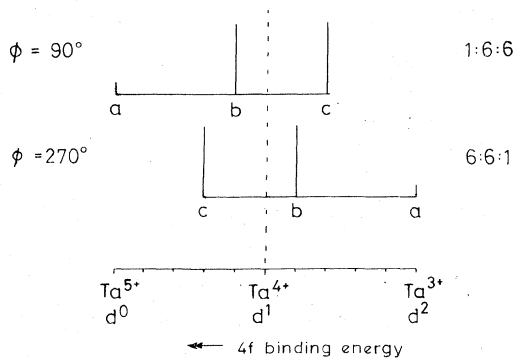


FIG. 16. Site-type populations and charge distributions for the $\sqrt{13}a_0$ triple-axis commensurate CDW, under the sine wave phasing choices of $\phi = 90^\circ$ and 270° . The amplitude of the CDW has been arbitrarily chosen to swing the *a* site valency by unity. The relative location of the sites on the charge scale is only approximate, in view of the appreciable cation sizes and shifts vis-à-vis λ (see Fig. 14).

(Note for 2*H*-TaSe₂, in the 1:6:1:1 situation of Fig. 3, the strong peak corresponds to $\delta\rho = 0$.)

For either phase choice it may seem rather a puzzle as to where the peak from the third site has vanished in the 1*T* spectra, since it should stand well clear of the two strong peaks. Again we shall see that this puzzle can be favorably resolved under the choice $\phi = 270^\circ$.

Even at 14 °K,⁶ where the CDW-induced splitting is fully developed, the third line is not apparent. It has been assumed, when making the 1:6:6 choice, that the third peak can be lost in the many-body tails, which stretch several eV above the strong line maxima. However, the resolution appears sufficient for this to be not so. Upon turning to the 6:6:1 choice, it initially appears that we are in a worse position, as the third peak now ought to stand out clear of the much sharper low-energy edge of the first strong peak. However, the model in assuming a linear shift in peak-position with CDW site-charge is over simple. First, there is the recognized neglect of any Madelung corrections to the peak positions from the CDW itself. Moreover, we have seen above that large in-plane cation shifts of $\frac{1}{4}$ Å occur. (The anions largely respond with bond-length-conserving *c*-axis motion.) It is evident that the most concerted effect falls on the symmetric center, site *a*. Under the choice $\phi = 270^\circ$, the effect acts to drive the weak line back the $\frac{1}{2}$ eV or somewhat more onto the first strong line. In fact, in Figs. 4 and 8 of Ref. 6 we are presented for 1*T*-TaS₂ with evidence of just such an effect. The first strong peak (i.e., of lowest binding energy) is found to be more intense than its partner to follow, despite the latter standing on the many-body tail of the former. With TaSe₂ this is not so immediately apparent because the peak separation is less (despite *T*₀ being higher), probably due to the ionicity decrease.

A final clue that the $\phi = 270^\circ$ choice is indeed the relevant one is supplied by XPS from Hf-substituted 1*T*-TaS₂ (3-at.%).⁶ In the Hf 4*f* spectrum, evidence of only a single site is obtained. This means that in the rather short coherence length situation which doping introduces, the Hf invariably can manage to be accommodated into the same type of siting. A hafnium atom would favor a rather low *d*-state content. This is readily secured in the six *c* sites of the 270° case, in contrast to persistently having to define the lone *a* siting, as in the 90° case.

It would be interesting at this point to have XPS results from TaTe₂ and distorted ReS₂, or from the singly-sited distortion of WTe₂ compared with undistorted WSe₂ and WS₂. However, ultimately, the best chance for outright resolution of this

problem would seem to lie in the ^{181}Ta Mössbauer measurements currently being attempted (see Ref. 37c), though counting statistics problems will be severe in the high-velocity region to be explored for site a with $\phi = 270^\circ$.

The existing Mössbauer data, secured by 1-at% ^{57}Fe substitutional doping of $1T\text{-TaSe}_2$, is fraught with interpretive problems.³⁷ The six Lorentzian least-squares fit to the data is not unique, and the final selection was made to match the XPS work and the presumed 1:6:6 result. The analysis led to a very wide spread in quadrupole splitting, which seems out of keeping with the distortions involved. Actually, it was found in the cases of heavier Fe doping (10–33-at.%), where the CDW is incommensurate and the Mössbauer spectrum simpler, that the low-temperature quadrupole splitting depends rather little on Fe concentration, despite significant lattice changes occurring. Seemingly unreasonable too in the 1% analysis is that the isomer shift for Fe in the a site should have a much *lower* isomer shift than in

$\text{Fe}_{1/3}\text{Ta}_{2/3}\text{S}_2$,³⁷ where all Ta sites are 5+. On a more fundamental level, it is still not clear to

what extent the Fe dopant atoms may be regarded as a passive gauge of the local charge distribution in the CDW. Is their valency an invariant 2+ at all concentrations, under total exclusion from rigid band formation?

VI. SUMMARY

A broadly based attempt has been made to secure understanding of the various forces at work that determine the structural forms actually acquired by the PSD's, through the set of electronically unstable $d^1\text{-}d^0$ dichalcogenides. Some of this work, especially for $2H\text{-TaSe}_2$, involves a matching of explanation to an already detailed bank of data. In other cases, as with NbTe_2 , it provides new guidelines, in a relatively little explored area. For $1T\text{-TaS}_2$ it produces a direct conflict with present understanding, if the CDW model, as seems most desirable, is to be retained for this material. Section IV highlights the soft mode condensation problem, common to all these triple-axis CDW materials.

- ¹D. E. Moncton, J. D. Axe, and F. J. DiSalvo, (a) Phys. Rev. Lett. **34**, 734 (1975); (b) Phys. Rev. B **16**, 801 (1977).
- ²J. A. Wilson, F. J. DiSalvo, and S. Mahajan, Adv. Phys. **24**, 117 (1975).
- ³*International Tables for X-ray Crystallography*, edited by N. F. M. Henry and K. Lonsdale (Kynoch, Birmingham, 1969), Vol. 1.
- ⁴(a) J. A. Holy, M. V. Klein, W. L. McMillan, and S. F. Meyer, Phys. Rev. Lett. **37**, 1145 (1976); (b) J. A. Holy, Ph. D. thesis (University of Illinois, Urbana, 1977) (unpublished).
- ⁵C. Berthier, D. Jerome, P. Molinie, and J. Rouxel, Solid State Commun. **19**, 131 (1976).
- ⁶H. P. Hughes and R. A. Pollak, Philos. Mag. **34**, 1025 (1976).
- ⁷J. A. Wilson, Phys. Rev. B **15**, 5748 (1977).
- ⁸G. K. Wertheim, F. J. DiSalvo, and S. Chiang, Phys. Rev. B **13**, 5476 (1976).
- ⁹F. Borsa, D. R. Torgeson, and H. R. Shanks, Phys. Rev. B **15**, 4576 (1977) (unfortunately not done with single crystals).
- ¹⁰R. Brouwer and F. Jellinek, Extended Abstracts, Fifth International Conference on Solid Compounds of Transition Metals, Uppsala, Sweden, June, 1976, p. 89 (unpublished).
- ¹¹J. A. Wilson and A. D. Yoffe, Adv. Phys. **18**, 193 (1969).
- ¹²B. Ricco, Solid State Commun. **22**, 331 (1977). [Note for all four compounds of the family, there is very little change in the band structure and Fermi surface—see G. Wexler and A. M. Woolley, J. Phys. C **9**, 1185 (1976).]
- ¹³C. W. Chu, V. Diatschenko, C. Y. Huang, and F. J.

- DiSalvo, Phys. Rev. B **15**, 1340 (1977).
- ¹⁴F. J. DiSalvo, D. E. Moncton, J. A. Wilson, and S. Mahajan, Phys. Rev. B **14**, 1543 (1976).
- ¹⁵R. A. Craven and S. F. Meyer (unpublished); and M. Barmatz, L. R. Testardi, F. J. DiSalvo, and J. M. E. Harper, Phys. Rev. B **13**, 4637 (1976).
- ¹⁶W. L. McMillan, Phys. Rev. B **14**, 1496 (1976).
- ¹⁷M. Barmatz, L. R. Testardi, and F. J. DiSalvo, Phys. Rev. B **12**, 4367 (1975).
- ¹⁸(a) C. S. Wang and J. M. Chen, Solid State Commun. **14**, 1145 (1974); (b) J. M. Chen and C. S. Wang, Solid State Commun. **14**, 857 (1974).
- ¹⁹(a) N. Wakabayashi, H. G. Smith, and R. Shanks, Phys. Lett. A **50**, 367 (1974); (b) N. Wakabayashi, H. G. Smith, and R. M. Nicklow, Phys. Rev. B **12**, 659 (1975).
- ²⁰S. K. Chen and V. Heine, J. Phys. F **3**, 795 (1973).
- ²¹J. A. Wilson and S. Mahajan, Commun. on Phys. **2**, 23 (1977). Recent modification of the original interpretation of the transition in TiSe_2 by R. M. White and G. Lucovsky, Il Nuovo Cimento B **38**, 280 (1977), is founded on faulty interpretation of the data they present in Fig. 1. The d band is lowered by Ti intercalation [see Ref. 32 and J. A. Wilson, *Proceedings of the International Conference on Lattice Dynamics* (Flammarion, Paris, 1977)]. With regard to the photoemission data quoted there, reference should be made to M. M. Traum, G. Margaritondo, N. V. Smith, J. E. Rowe, and F. J. DiSalvo (unpublished).
- ²²J. A. Wilson, Phys. Status Solidi B **86**, 11, (1978); Solid State Commun. **22**, 551 (1977).
- ²³F. J. DiSalvo, D. E. Moncton, and J. V. Waszczak, Phys. Rev. B **14**, 4321 (1976).
- ²⁴R. Dupree, W. W. Warren, and F. J. DiSalvo, Phys.

- Rev. B 16, 1001 (1977).
- ²⁵M. Barmatz, R. Farrow, and F. J. DiSalvo (unpublished).
- ²⁶A. M. Woolley and G. Wexler, J. Phys. C 10, 2601 (1977).
- ²⁷F. J. DiSalvo and J. V. Waszczak, J. Phys. (Paris) 37, C 4-157 (1976); M. Bayard and M. J. Sienko, J. Solid State Chem. 19, 325 (1976); C. F. van Bruggen and C. Haas, Solid State Commun. 20, 251 (1976).
- ²⁸N. V. Smith and M. M. Traum, Phys. Rev. B 11, 2087 (1975).
- ²⁹Among the *unrotated* hexagonal superlattices, centroid sites *B* and *C* are cation sites (as *A*) only for $a = 3na_0$. For rotated superlattices up to $8a_0$ this is so only for cell sides $\sqrt{21}a_0$, $\sqrt{39}a_0$, $\sqrt{57}a_0$, and $\sqrt{63}a_0$, with edge rotations of 4 by 1, 5 by 2, 7 by 1, and 6 by 3, respectively. We see $\sqrt{13}a_0$, $4a_0$, and $\sqrt{19}a_0$ are excluded from this group.
- ³⁰J. van Landuyt, G. van Tendeloo, and S. Amelinckx, Phys. Status Solidi A 29, K11 (1975); see, also, S. Amelinckx J. Phys. (Paris) 37, C4-83 (1976).
- ³¹D. E. Moncton, F. J. DiSalvo, J. D. Axe, L. J. Sham, and B. R. Patton, Phys. Rev. B 14, 3432 (1976).
- ³²F. J. DiSalvo, J. A. Wilson, B. G. Bagley, and J. V. Waszczak, Phys. Rev. B 12, 2220 (1975).
- ³³J. A. Wilson, (a) Adv. Phys. 21, 143 (1972); (b) *Proceedings of the Conference on Phase Transitions*, edited by L. E. Cross (Pergamon, New York, 1973), pp. 101-115.
- ³⁴H. F. Franzen, C. Haas, and F. Jellinek, Phys. Rev. B 10, 1248 (1974).
- ³⁵F. Hulliger, Struct. Bonding (Berlin) 4, 83 (1968).
- ³⁶S. H. Liu, Phys. Rev. B 10, 3619 (1974).
- ³⁷M. Eibschütz and F. J. DiSalvo, Phys. Rev. B 15, 5181 (1977); Phys. Rev. Lett. 36, 104 (1976). Also, L. Pfeiffer, M. Eibschutz, and D. Salomon, Fourth International Conference on Hyperfine Interactions, Madison, N. J., June, 1977 (unpublished).
- ³⁸T. Butz, A. Vasquez, H. Ernst, and A. Lerf, Phys. Lett. A 58, 51 (1976).
- ³⁹Y. Yamada and M. Takatera, Solid State Commun. 21, 41 (1977).
- ⁴⁰A. Kotani, J. Phys. Soc. Jpn. 42, 408, 416 (1977); 42, 416 (1977).